Nonmonotonic Size Dependence in the Hole Mobility of Methoxide-Stabilized PbSe Quantum Dot Solids

Marcus Scheele,[†,‡] Jesse H. Engel,[†,‡] Vivian E. Ferry,[†,‡] David Hanifi,[§] Yi Liu,[§] and A. Paul Alivisatos[†,‡,*]

[†]Material Sciences Division, Lawrence Berkeley National Laboratory, Berkeley, California 94720, United States, [‡]Department of Chemistry, University of California, Berkeley, California 94720, United States, and [§]Molecular Foundry, Lawrence Berkeley National Laboratory, Berkeley, California 94720, United States

ABSTRACT We present a facile procedure to fabricate p-type PbSe-based quantum dot solids with mobilities as large as 0.3 $cm^2 V^{-1} s^{-1}$. Upon partial ligand exchange of oleate-capped PbSe quantum dots with the methoxide ion, we observe a pronounced red shift in the excitonic transition in conjunction with a large increase in conductivity. We show that there is little correlation between these two phenomena and that the electronic coupling energy in PbSe quantum dot solids is much smaller than often assumed. However, we observe for the first time a nonmonotonic size dependence of the hole mobility, illustrating that coupling can nonetheless be dominant in determining the transport characteristics. We attribute these effects to a decrease in charging energy and interparticle spacing, leading to enhanced electronic coupling on one hand and enhanced dipole interactions on the other hand, which is held responsible for the majority of the red shift.

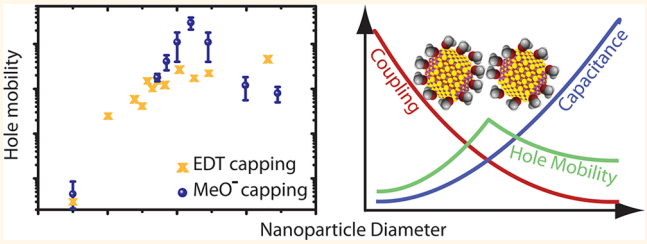

KEYWORDS: quantum dot solids · electrical transport · optical properties · coupling

Quantum dot solids (QDS) made from PbSe nanoparticles have led to a variety of (opto-)electronic applications ranging from field-effect transistors (FET) and thermoelectrics to photodetectors and solar cells.[1,2] Electrical transport in these artificial solids has been well described as a network of spatially and energetically disorder hopping sites, where the mobility is determined by an interplay between electronic coupling, interparticle spacing, charging energy, and energetic polydispersity.[3] To increase the conductivity in PbSe QDS, numerous techniques have been developed, employing small cross-linkers such as hydrazine, alkanedithiols, ethylenediamine, thiocyanate, *N,N'*-dimethylformamide/tetrafluoroborate, sulfide, dicarboxylic acids, and halogenides.[1,4–6]

Theoretically, it has been shown that as nanoparticle size is decreased, a fundamental trade-off exists between promoting transport through increased electronic coupling from enhanced wave function overlap and inhibiting transport through increased charging energy from a smaller self-capacitance.[7] This trade-off has been suggested as an explanation of nonmonotonic size-dependence of mobility in systems with sufficient electronic coupling, such as electron transport in ethanedithiol (EDT)-capped PbSe QDS.[8,9] Here, we observe for the first time a nonmonotonic size-dependence of the hole mobility in QDS, by investigating methoxide-stabilized PbSe nanoparticles. We attribute this behavior to the shorter interparticle spacing, which results in an increase in hole tunneling probabilities and a decrease in charging energy. Typically, ligand exchange with a short cross-linker results in an optical red shift of the $S_e \leftarrow S_h$ transition as well as an enhancement in the field-effect mobility. These processes are usually completed within seconds and therefore difficult to resolve in time.[4] Here, we study the shift of these two parameters after ligand exchange with a short cross-linker and its reversal upon exposure to air. Both parameters decay on very different time scales, indicating a lack of correlation between the optical shift and the change in field-effect mobility. We conclude that the induced red shift cannot be primarily due to electronic coupling.

RESULTS

The eight PbSe quantum dot (QD) samples analyzed in this study are characterized

* Address correspondence to alivis@berkeley.edu.

Received for review April 4, 2013 and accepted July 16, 2013.

Published online July 16, 2013
10.1021/nn401657n

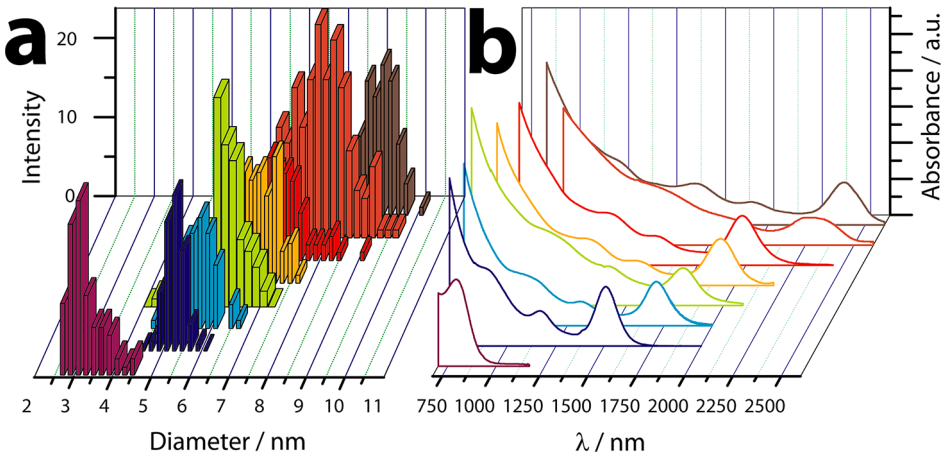

Figure 1. Characterization of the eight PbSe nanoparticle samples studied in this work. Transmission electron microscopy (TEM) was used to derive the mean particle diameter and size distribution of at least 100 particles per sample. UV−vis spectroscopy was applied to correlate the mean particle diameter to the energy of the $1S_e \leftarrow 1S_h$ transition of each sample.

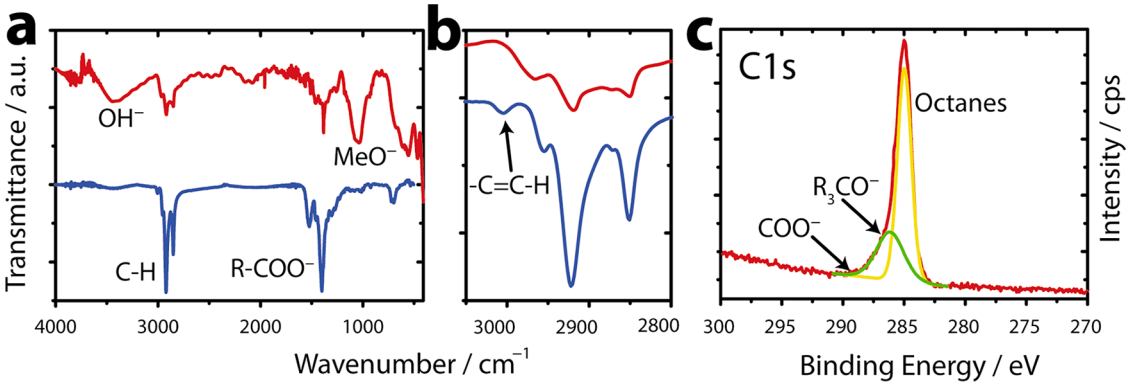

Figure 2. Effect of ligand exchange of 6.4 nm PbSe nanoparticles with MeO^-. (a) FT-IR reveals that the particles are initially capped with oleate (blue) as indicated by the strong C−H stretching bands at 3000 cm^{-1},the C═C stretching band at >3000 cm^{-1}, and the weakened C═O stretching band at 1400 cm^{-1}, which is significantly removed upon ligand exchange (red). (b) FT-IR scan of the C−H stretching mode region. (c) X-ray photoelectron spectroscopy of the C 1s core level with raw data displayed in red. The yellow and green lines represent two Gaussian−Lorentzian fits centered at about 285.0 and 286.4 eV, respectively.

in terms of size, size distribution, and optical absorption in Figure 1 and show $S_e \leftarrow S_h$ transition energies in accordance with previous observations.[10,11]

To fabricate cross-linked QDS, we apply a 5.0 mM solution of tetrabutylammonium hydroxide (TBA-OH) in methanol to spin-cast thin films. The solution is described by the equilibrium

$$H_3C—OH + HO^- \rightleftarrows H_3C—O^- + H_2O$$

Following the law of mass action, it is straightforward to show that in a 5 mM solution of TBA-OH in methanol the molar ratio of CH_3O^- to OH^- will be 95:1. From here on, we will refer to the capping ligand introduced by this treatment as "methoxide (MeO^-)", although the exchange solution contains 1% OH^- as an impurity. For more details, the reader is referred to the Supporting Information (SI).

Exposing a thin film of Pb-oleate-capped PbSe nanoparticles to MeO^- leads to instantaneous insolubility of the particle film in nonpolar solvents such as hexanes or chloroform. FT-IR (Figure 2, exemplarily shown for 6.4 nm particles before and after ligand exchange) indicates the change in chemical nature of the ligand shell upon this treatment. The broad band at 3500 cm^{-1} is indicative of an OH-containing species, whereas the band at 1100 cm^{-1} is typical for the methoxide ion. The same species causes the multiple C−H stretching bands at <3000 cm^{-1} and the sharp peak at 1380 cm^{-1}. In the spectrum of the original Pb-oleate ligand we note two characteristic features of the C═O stretching bands between 1400 and 1500 cm^{-1} (indicating a binding interaction) and the small C═C band at 3010 cm^{-1}. Both features vanish upon treatment with MeO^- (the most energetic C−H feature in this spectrum occurs at 2970 cm^{-1}), which we attribute to an at least partial ligand exchange.

The extent of ligand exchange is further validated by X-ray photoelectron spectroscopy (XPS) of the same particle sample in the energy regime of the C 1s level. Where previous studies of Pb-oleate-capped nanoparticle films clearly resolved a COO^- feature at 288 eV in XPS, this feature is absent after treatment with MeO^- and

supports the conclusion of a partial ligand exchange.[4] We note that the C 1s signal cannot be described adequately with a single Gaussian–Lorentzian component but rather requires a second function at higher energy centered at about 286.2 eV. We interpret the first signal with residual hexanes/octane adsorbed by the film and the second signal with the carbon in the methoxide ion. Note that the 1s core level of R_3C-O is expected at 286.4 eV.[12]

Thin films of all oleate-capped samples have the same $S_e \leftarrow S_h$ transition energy as the colloidal sample in tetrachloroethylene. Upon MeO^- treatment, all QD samples exhibit a pronounced red shift consistent with results for hydrazine-, ethanedithiol-, or dicarboxylic acid-capped PbSe QDS.[1,4,13,14] As demonstrated in Figure 3a the red shift upon ligand exchange increases with decreasing particle size. For the smallest particles (3 nm), the exciton was not measurable in thin films, possibly due to either extremely large exciton shifts or the dominance of Fabry–Pérot cavity modes.[2] For more details on these arguments, the reader is referred to the SI. For comparison, we include two reference points for EDT-capped PbSe nanoparticles at a given size in the diagram.[4,8] It is apparent that the size-dependence of the shift in $S_e \leftarrow S_h$ transition energy upon ligand exchange with MeO^- or EDT is very similar for both systems. The shift is found to be highly sensitive to oxidation, to the point that the red shift experiences an oxygen-induced blue shift of equal and opposite magnitude within the first 2 min of exposure to air (Figure 3b). Previous studies using carboxylic acids and PbSe have found similar quick reversals of excitonic red shift upon air exposure.[13]

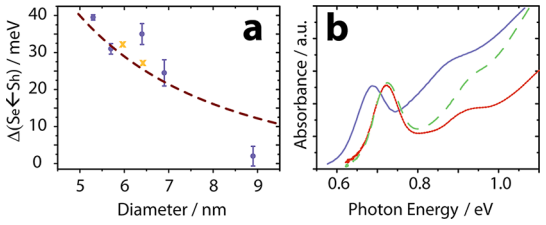

Figure 3. (a) Size-dependence of the optical shift of the $1S_e \leftarrow 1S_h$ transition in PbSe nanoparticle films on ligand exchange from $Pb(oleate)_2$ to $Pb(MeO)_2$ (blue dots) or Pb(ethandithiolate) (orange crosses). Error bars are standard deviations from three samples. Values for exchange with Pb(ethanedithiolate) were reproduced from ref 4. The dashed line respresents simulated optical shifts from dipole–dipole coupling. (b) Vis–IR spectra of the same PbSe sample capped with $Pb(oleate)_2$ (red dotted line), with $Pb(MeO)_2$ under argon (blue solid line), and with $Pb(MeO)_2$ after 2 min in air (green dashed line).

We demonstrate the reduction of interparticle spacing upon ligand exchange from $Pb(oleate)_2$ to $Pb(MeO)_2$ by a comparative TEM study in Figure 4. Films of initially well-dispersed quantum dots with a mean interparticle spacing of roughly 15 Å undergo a contraction to ~2–3 Å upon exchange with methoxide. We note a similar effect reported in PbSe nanoparticle films where hydrous methanol was used to replace $Pb(oleate)_2$.[15] In that work, partial fusion of nanoparticles was reported upon ligand exchange, which we do not observe with the treatment presented here.

We further investigate the effect of MeO^- stabilization on PbSe QDS by field-effect transistor measurements. Initially insulating $Pb(Oleate)_2$-capped PbSe nanoparticle films become conductive upon methoxide exchange for all samples, with conductivities (σ) as high as 0.05 S cm^{-1} (d = 6.4 nm). A representative source–drain sweep and transconductance sweep are presented in Figure 5.

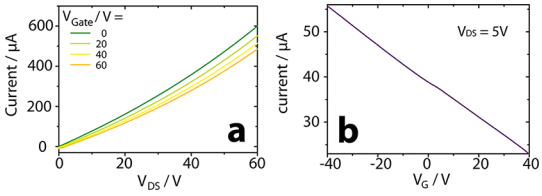

Figure 5. Field-effect transistor characteristics for a 6.4 nm MeO^--capped PbSe QDS. (a) Positive drain sweep with 0, 20, 40, and 60 V gate voltages applied. (b) Transfer curve of the same film at 5 V source–drain bias.

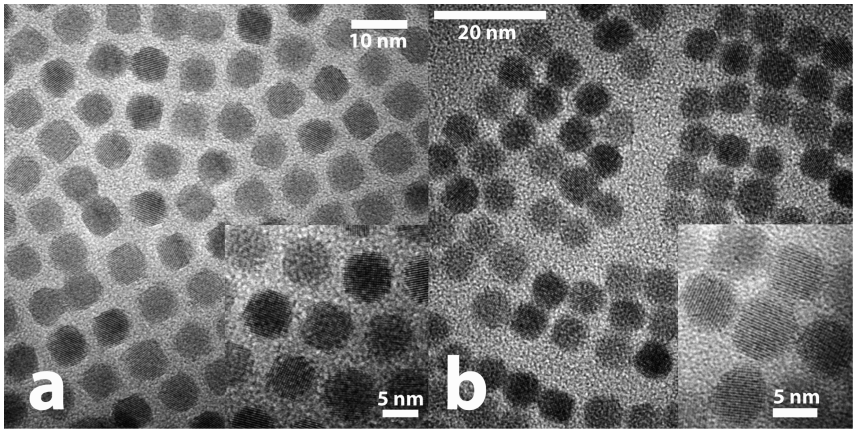

Figure 4. TEM images of monolayers of PbSe nanoparticles capped with $Pb(oleate)_2$ (a) or $Pb(MeO)_2$ (b). The insets represent images of the same sample at higher magnifications.

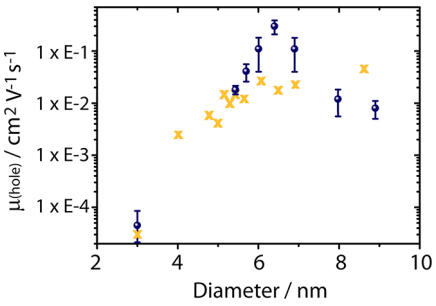

Figure 6. Size-dependent field-effect hole mobilities of PbSe quantum dot solid films. (Blue circles) Particles capped with $Pb(MeO)_2$. Error bars are standard deviations from at least three different devices. (Orange crosses) Particles capped with Pb(ethandithiolate); values reproduced from ref 8.

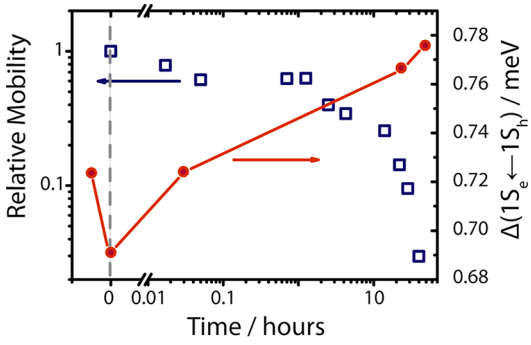

Figure 7. (Semi)log plot of the time-dependent oxidation of 5.7 nm PbSe quantum dots capped with $Pb(MeO)_2$. The dashed line marks the time after ligand exchange at the instant of exposure to air. (Blue squares, left axis) Degradation of the hole mobility. (Red dots, right axis) Change of the $1S_e \leftarrow 1S_h$ transition energy. The solid line serves as guidance to the eye.

The negative slope of the transconductance sweep (Figure 5b), that is, the decrease in drain current upon increased electron injection, is indicative of unipolar hole transport and p-type behavior. We extract the field-effect hole mobilities (μ_h) in the linear regime and derive the hole concentration (n_h) *via* Ohm's law [see SI]. We find n_h to be relatively constant, having a concentration of $(8 \pm 2) \times 10^{17}$ cm^{-3} over the whole size regime studied.

In Figure 6, we display the size-dependent field-effect hole mobility. For comparison, we plot μ_h over the same PbSe diameter range as for EDT-capped PbSe QDS taken from ref 8. As explained therein, μ_h increases monotonically with size. In contrast, for MeO^- capping we find a nonmonotonic size-dependence for the hole mobilities with a maximum at $d = 6.4$ nm, exceeding μ_h for EDT capping of this particle size by over 1 order of magnitude.

Upon exposing transistors of MeO^--capped PbSe QDS to air, μ_h is found to decrease slowly over the course of hours and days. We demonstrate this exemplarily for 5.7 nm particles in Figure 7 but note a similar behavior for all sizes. We simultaneously plot the change in $S_e \leftarrow S_h$ transition energy over the same time interval. After an initial red shift due to the ligand exchange, upon air exposure the transition energy gradually blue shifts at a much slower rate, consistent with previous reports.[4,14]

DISCUSSION

The technique presented here provides a facile way to prepare p-type PbSe QDS with large mobilities at high doping levels. This material has potential for application as a thin-film thermoelectric where unipolar transport, large mobilities, and carrier concentrations of 10^{18} cm^{-3} are ideal. The preserved quantum confinement and nanostructure with subphonon wavelength grain sizes hold for additional improvements of the Seebeck coefficient and reduction of thermal conductivity.[16,17] We would like to emphasize that the procedure presented here does not involve annealing in air or other less controlled oxidation techniques applied previously.[6,18] Rather, the carrier concentration is fixed after brief exposure (~3 s) to the ligand exchange solution. When kept under inert conditions, MeO^--capped PbSe QDS exhibit stability of optical and electrical properties for weeks. In contrast with a similar report on ligand exchange with hydrous methanol, we do not observe significant changes in particle size and morphology.[15] We attribute this to the relatively acidic conditions imposed by hydrous methanol, which is known to facilitate the fusion of particles *via* oriented attachment in lead chalcogenide nanostructures.[17] In contrast, the method presented here imposes basic conditions and short exposure times, which minimizes the probability of etching and fusion.

Increased Hole Mobility over EDT Capping and Nonmonotonic Size-Dependence. Transport through a QDS is determined by the interplay between electronic coupling and the activation energy for interparticle hopping.[19] We consider three explanations for the greater hole mobilities observed for MeO^- capping *vs* EDT capping: (1) a decrease of the activation energy due to an increase of the effective static dielectric constant of the ligand matrix, (2) an increase of electronic coupling, and (3) a smaller surface trap state density.

The activation energy is the sum of the charging energy E_C and the site disorder $\Delta\alpha$. Kang *et al.* demonstrated that the room-temperature activation energy of PbSe FETs could be well accounted for through nearest-neighbor hopping models, with six nearest neighbors. These models assume two-dimensional transport, as the injected carriers lie in a plane at the gate oxide interface.[19] Under this assumption, the site disorder can be approximated from the full-width half-maximum (fwhm) of the $S_e \leftarrow S_h$ transition as

$$\Delta\alpha = 0.43 \text{ fwhm}/(4\sqrt{2 \times \ln \times 2})$$

and the charging energy can be calculated by applying a modified Laikhtman–Wolf model, which takes into account the mutual capacitance of nearest neighbors and the effective dielectric constant of the total medium

(nanoparticles, ligands, and voids).[20−22] The full details of these calculations are given in the SI, and it is interesting to note that we arrive at similar values of the charging energy for both the nearest-neighbor calculations and the Laikhtman−Wolf model.

We find the charging energy to be a stronger function of ligand permittivity than interparticle spacing. Assuming the same static dielectric constant of the ligand (ε_L), we calculate comparable values for the charging energy of EDT- and MeO^--capped particles, despite the differences in interparticle spacing (2−3 vs 5 Å).[19] In contrast, large differences in E_C are observed when changing the static dielectric constant. For a 5.7 nm PbSe particle for instance, E_C decreases from 9.3 meV to 2.1 meV upon changing ε_L from 2.6 (as in $Pb(EDT)_2$ capping) to 10. Although ε_L of $Pb(MeO)_2$ is unknown, we conclude that one possible explanation for the larger mobilities of PbSe films capped with MeO^- *vs* EDT could be a larger static dielectric constant of the ligand.

We now consider increased electronic coupling as the reason for improved transport. As demonstrated in ref 8, the mobility of PbSe nanoparticle films is well described by the Miller−Abrahams expression such that the tunneling rate depends on $\exp(-\beta d)$, where d is the interparticle spacing and β is a constant that depends on the carrier effective mass and the height of the tunneling barrier. Since β is on the order of 1 $Å^{-1}$, a change in d from 5 Å to 2−3 Å invokes a significant increase (7−20 times) in the tunneling rate, and we note that the upper end of this range approximately matches the difference in carrier mobility observed for 6.4 nm diameter particles, where mobilities are at their peak.[9]

Lastly, efficient surface passivation and small trap state densities in PbSe QDS have been shown to result in drastically improved mobilites.[23] Since methoxide capping of PbSe leads to a larger carrier concentration than capping with EDT, such an effect is unlikely to be responsible for the increased mobility in the present case. Given the low values of charging energy and the large increase in tunneling probabilities, we attribute the improved transport properties predominantly to increased electronic coupling.

Electronic coupling and the activation energy to transport both decrease monotonically with increasing nanoparticle diameter. This is due to the reduction in particle−particle wave function overlap and a growing self-capacitance, respectively.[9] In many systems, electronic coupling is so small that changes in activation energy are always the limiting factor, and the size-dependent mobilities follow it monotonically. When both parameters are of comparable magnitude, their competition can result in a nonmonotonic size-dependence of the carrier mobility.[9] For PbSe, this has first been observed by Liu *et al.* for electrons in EDT-capped nanoparticles.[8] However, the corresponding hole mobility was seen to increase monotonically with size. This has recently been explained with different coupling strengths of electrons and holes under the assumption that holes carry a larger effective mass in EDT than electrons.[9] The fact that MeO^--capped PbSe nanoparticle films exhibit a nonmonotonic size-dependence of the hole mobilities (see Figure 6) highlights our conclusion that electronic coupling is significantly improved over EDT capping, in conjunction with a decrease in the activation energy. There may exist a similar increase in electron mobilities as well; however we were not able to measure these values for the moderately doped and unipolar MeO^- transistors. We note that a third factor for the observed size-dependence of the mobilities could be a size-dependent trap state density. For example, small, octahedral lead chalcogenide nanoparticles are typically more stable toward oxidation than larger, more cuboctahedral-shaped particles.[24] The latter type of particles is more likely to possess a large number of surface states for this reason, which may explain the relatively low mobility of the largest PbSe sample in the present work. However, such a size-dependence is not reflected in the carrier concentrations, which are constant over the whole range of particle samples.

Finally, it is noteworthy that despite the seemingly improved electronic coupling for MeO^- *vs* EDT capping, the size-dependence of the optical red shift is very similar for the two systems (Figure 3a). This provides supporting evidence that there is little correlation between the red shift and the degree of electronic coupling in these materials.

Correlation between Optical Shift and Field-Effect Mobility. The origin of this optical shift has previously been attributed to three components: (1) electronic coupling, (2) polarization effects, and (3) transition dipole−transition dipole coupling.[4,12,25−27]

We stress an important difference in the treatment of the dielectric environment between electric and optical problems: Whereas for electric particle−particle interactions the static dielectric constant, that is, the real part of the dielectric function at low frequencies has to be considered, for optical interactions, it is the complex dielectric function at optical frequencies that is most relevant.[28]

Calculations have shown that a sizable amount of electronic coupling is necessary to overcome the charging energy inherent to QDS and explain the observed mobilities, but the magnitude varied between 10 meV and 8 μeV for the same system depending on the calculation.[3,9] Strong polarization effects can result from a mismatch of optical dielectric constants at the interface between nanoparticle and ligand; however previous studies have shown such effects to be significantly smaller than the observed shifts.[25,29] We also find only small shifts (1−5 meV) when applying such calculations to our data. Finally, transition dipole−transition dipole coupling could possibly explain a red shift of similar magnitude for CdS clusters.[26,30]

In a similar manner, here we explore a classical coupled dipole−dipole model and find that it explains the majority of the observed shift in the MeO^--capped films (dashed line in Figure 3a). In short, we consider the coupling of transition dipoles embedded within a dielectric surrounding defined by the Maxwell−Garnett effective media approximation.[28,31] While a complete coupled dipole model uses spectrally dependent optical dielectric constants, the version used here is a simplified model that assumes nondispersive properties of both the nanoparticle and ligand. We check this assumption by utilizing the Kramers−Kronig relations to extract optical permittivities from the solution-phase measurements and find that they remain relatively constant (24 ± 1) over the range of optical wavelengths. Complete details of these calculations are given in the SI. We also note that the negligible red shift of the largest particles is far less than expected. This may point to the inadequacy of the various assumptions within the model, such as a constant optical dielectric value, the permittivity of the ligand, the packing fraction of the spheres, the validity of Maxwell−Garnett effective media theory, or the absence of quantum mechanical treatments.

The complete recovery of the original absorption spectrum of oleate-capped QDs upon (1) exchange with MeO^- and (2) exposure to air for 2 min as displayed in Figure 3b has the following implications:

(a) The optical shift is not caused by partial sintering, necking, or ripening as recently put at question since such effects are unlikely to be reversed on brief exposure to air.[3]

(b) There is little correlation between the optical shift and the field-effect mobility. As demonstrated in Figure 7, the deterioration of μ_h upon exposure to air happens on a much longer time scale. Where the optical shift has completely vanished after 2 min of air exposure, the mobility decreases by less than 40% in the same time. Notable changes in μ_h appear after several hours, but at this point the $S_e \leftarrow S_h$ transition energy of MeO^-- and oleate-capped QDS alike have blue-shifted significantly, which is indicative of the formation of an oxide shell.[14]

Hence, our data support the view that electronic coupling is only weakly reflected in the red shift but almost entirely due to transition dipole coupling or polarization effects.

Reversal of the Optical Red Shift upon Exposure to Air. Oxidation of PbSe in air is a multistep process leading to the formation of PbO, $Pb(OH)_2$, and $PbSeO_x$ species.[4,32] O_2 is readily incorporated into the PbSe lattice, resulting in a smaller semiconductor nanoparticle diameter and larger interparticle spacing. This oxidation is rapid in the beginning but slows down considerably as the oxide shell growth proceeds.[32,33] Water can have a similarly

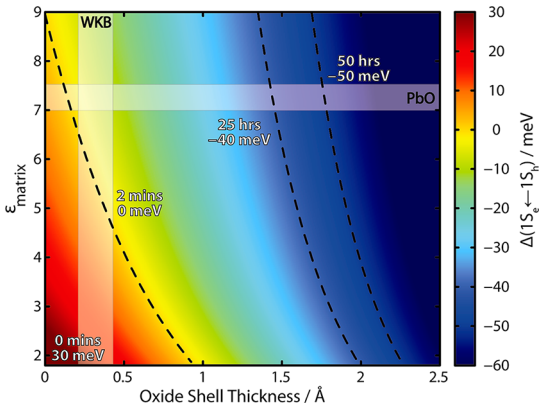

Figure 8. Simulation of the optical shift of the 5.7 nm MeO^--capped PbSe nanoparticle QDS from Figure 7. The shift is parametrized as a function of the matrix permittivity and the thickness of an oxide shell covering each nanoparticle. A 0 meV shift means the energy of the oleate-capped QDS before exchange with MeO^- and exposure to air (722 meV). At time t = 0 min (the instant of exposure to air), the red shift is +30 meV, the oxide shell thickness is 0 Å, and the dielectric of the matrix is assumed to be 1.8. The three dashed lines relating exposure time to the excitonic red shift are taken from Figure 7. The vertical white overlay represent a range of possible values for oxide shell-thickness after two minutes air exposure based on using the WKB approximation to explain the observed mobility decrease. The horizontal white overlay represents a range of matrix permittivity values if the surface and void space were completely filled with PbO.

detrimental effect on the structure and chemical nature of PbSe by substitutional incorporation into the lattice and formation of H_2Se and $Pb(OH)_2$. For example, Zhang *et al.* have studied the gradual formation of an amorphous $Pb(OH)_2$ shell onto the surface of PbTe nanoparticles upon exposure to aqueous bases.[34] Specifically in the case of MeO^--capped nanoparticles, exposure to moisture will lead to the formation of methanol in the ligand sphere. In Figure 8, using the same coupled dipole−dipole model, we consider two different explanations for the rapid reversal of the optical red shift in MeO^--capped PbSe nanoparticles upon exposure to air as displayed in Figure 7: (1) a change in the dielectric environment inflicted by oxidation of the nanoparticle, and (2) a change in nanoparticle diameter due to the oxide shell.

The permittivity of the ligand/void matrix depends upon the permittivities of each of the possible oxidation products and their respective filling fraction. Given the diversity of possible oxidation products, we decided to parametrize the red shift simply in terms of the effective permittivity of the ligand matrix after oxidation. Starting from the permittivity of methanol (∼1.8) at optical frequencies, an increase to 9 upon exposure to air would be required to solely explain the red shift reversal. At the same time, we note that increasing quantum confinement and reducing the polarizability volume by the formation of a 0.9 Å thick oxide shell could account for the shift without changing the matrix optical dielectric constant. The realistic

TABLE 1. Specific Amounts and Times for Individual Particle Size Fractions of PbSe QDs

particle size/nm	m(PbO)/ mg	V(oleic acid)/ mL	V(ODE)/ mL	V(TOP-Se)/ mL	reaction time/s	DPP added?
3.0	223	0.8	20		90	
5.3	1090	3.8	17	15 (1.9 M)	60	yes
5.7	540	2.0	4.0	4.8	40	yes
6.0	294	2.0	3.0	3.0	90	no
6.4	405	1.5	5.0	3.6	40	yes
6.9	405	1.5	3.0	2.6	40	yes
7.9	298	1.6	3.0	3.0	150	no
8.9	270	1.0	3.3	3.8	120	no

situation probably lies somewhere between these two extremes, and we note that using the WKB approximation, the mobility decrease of 40−60% experienced over the same initial oxidation would correspond to an increased edge−edge interparticle distance of 0.5−0.9 Å or the formation of a 0.25−0.45 Å thick oxide shell. This would leave a value of the matrix permittivity roughly between 4.5 and 6, which is in relatively good agreement with the values for PbO.[35,36] For longer oxidation times, the matrix dielectric has less effect on the excitonic shift, and the model predicts the formation of much thicker oxide shells, which would correspond to the significant decline in mobility.

CONCLUSION

We have investigated the correlation between the optical shift of the $S_e \leftarrow S_h$ transition and the field-effect mobility in methoxide-capped PbSe quantum dot solids. By studying their degradation in air, we find both processes to be weakly correlated, which implies that the actual coupling energy responsible for the observed hole mobilities of up to 0.3 $cm^2\ V^{-1}\ s^{-1}$ is much smaller than often assumed. Nonetheless, coupling is found to be competitive with the activation energy to transport, as evident by the nonmonoticity in the size-dependent hole mobilities. On using an effective medium approach, we achieved reasonable agreement between our optical data and the shift predicted due to dipole−dipole interactions upon changing the dielectric environment and interparticle spacing by ligand exchange and oxidation in air.

METHODS

Synthesis of PbSe Nanoparticles. PbSe nanocrystals were synthesized by slightly modifying previously reported procedures.[1,2] All manipulations were carried out in a dry and oxygen-free environment. Specific amounts and times for individual particle sizes are reported in Table 1.

Lead(II) oxide (Aldrich, 99.999%) was mixed with oleic acid (Aldrich, 90%) and 1-octadecene (ODE) (Aldrich, 90%) in a three-necked flask with a temperature couple control finger, reflux condenser, and septum and heated under vacuum to 100 °C for at least 90 min, by which a colorless solution was obtained.

For the synthesis of 3.0 nm nanoparticles, we followed the procedure developed by Ma *et al*. A solution of 68 μL of bis(trimethyl)silylselenide in 3.0 mL of ODE was used as the selenium precursor. The reaction temperature was 130 °C.

For all other particles, we used a 1.0 M TOP-Se solution (1.9 M for the 5.3 nm sample), obtained by dissolving 1.185 g (2.2 g) of selenium powder (Aldrich, 99.99%) in 15.0 mL of trioctylphosphine (TOP) (Strem Chemicals, >97%) on stirring for 2 h. For some particles used in this work, 130 μL of diphenylphosphine (DPP) (Aldrich, 98%) was added to the solution. The solution containing the lead precursor was set in an argon atmosphere and heated to 180 °C. The TOP-Se solution was rapidly injected, upon which the solution temperature dropped to 155−160 °C, and the heater was switched off.

For all particles after the desired reaction time had passed, 10 mL of cold hexanes was carefully injected, and the solution was additionally cooled with an external water bath.

The nanocrystals were precipitated by the addition of anhydrous ethanol, the suspension was centrifuged for 5 min at 4500 rpm, the supernatant was discarded, and the precipitate was dissolved in anhydrous toluene. It was washed two more times on adding anhydrous methanol and one more time with acetone. Finally the nanocrystals were stored in a 9:1 mixture of anhydrous hexanes/octane.

Ligand Exchange with Tetrabutylammonium Hydroxide. Substrates were cleaned on using soap scrub and rinsing with distilled water, followed by 2-propanol and acetone, blow-dried and plasma-cleaned for 5 min, and mounted onto a spin-coater. While spinning at 2000 rpm, one drop of a filtered hexanes/octane (9:1) solution of nanoparticles (roughly 10 mg/mL) was drop-cast onto the substrate, followed by 30 μL of a filtered 5 mM solution of tetrabutylammonium hydroxide in methanol, three consecutive drops of methanol to spin-off excess ligand, and, finally, three consecutive drops of hexanes to wash off the oleate. This procedure was repeated until a thickness of roughly 50 nm was reached as determined from ellipsometry.

Conflict of Interest: The authors declare no competing financial interest.

Supporting Information Available: Description of characterization methods. Calculation of the ratio between methoxide and hydroxide concentrations. Description of the dipole−dipole model, calculation of the charging energy, description of the Kramers−Kronig transform, and simulation of Fabry−Perot modes in thin films of 3.0 PbSe quantum dots. Figures of (S1) estimation of the size dependence of the static dielectric constant of PbSe, (S2) simulation of charging energies, (S3) comparison of charging energies calculated by the Laikhtman−Wolf *vs* nearest-neighbor hopping model, (S4) calculation of activation energies to transport, (S5−8) application of Kramers−Kronig transform to 5.7 nm PbSe nanoparticles capped with $Pb(oleate)_2$ in solution to extract the real optical permittivity, (S9−12) extraction of n,k of 3.0 nm PbSe quantum dots, prediction of the thickness-dependent absorption of thin films, and comparison with experiment. This material is available free of charge *via* the Internet at http://pubs.acs.org.

Acknowledgment. Nanoparticle synthesis and characterization, ligand exchange, sample preparation, and transport measurements were funded by the Self-Assembly of Organic/Inorganic Nanocomposite Materials program (Grant DE-AC02-05CH11231 to A.P.A), photoelectron spectroscopy experiments were carried out within the Helios Solar Energy Research Center, and FT-IR spectroscopy was performed as a User Project at the Molecular Foundry, Lawrence Berkeley National Laboratory, all of which are supported by the Director, Office of Science, Office of Basic Energy Sciences of the U.S. Department of Energy under Contract No. DE-AC02-05CH11231. M.S. would like to thank the Alexander von Humboldt Foundation for a Feodor Lynen Fellowship. David K. Britt is acknowledged for providing the 5.3 nm nanoparticle sample and Waqas Khalid for fabricating the FET substrates used in this work.

REFERENCES AND NOTES

1. Talapin, D. V.; Murray, C. B. PbSe Nanocrystal Solids for n- and p-Channel Thin Film Field-Effect Transistors. *Science* **2005**, *310*, 86–89.
2. Ma, W.; Swisher, S. L.; Ewers, T.; Engel, J.; Ferry, V. E.; Atwater, H. A.; Alivisatos, A. P. Photovoltaic Performance of Ultrasmall PbSe Quantum Dots. *ACS Nano* **2011**, *5*, 8140–8147.
3. Guyot-Sionnest, P. Electrical Transport in Colloidal Quantum Dot Films. *J. Phys. Chem. Lett.* **2012**, *3*, 1169–1175.
4. Luther, J. M.; Law, M.; Song, Q.; Perkins, C. L.; Beard, M. C.; Nozik, A. J. Structural, Optical, and Electrical Properties of Self-Assembled Films of PbSe Nanocrystals Treated with 1,2-Ethanedithiol. *ACS Nano* **2008**, *2*, 271–280.
5. Nag, A.; Kovalenko, M. V.; Lee, J.-S.; Liu, W.; Spokoyny, B.; Talapin, D. V. Metal-Free Inorganic Ligands for Colloidal Nanocrystals: S^{2-}, HS^{-}, Se^{2-}, HSe^{-}, Te^{2-}, HTe^{-}, TeS_3^{2-}, OH^{-}, and NH_2^{-} as Surface Ligands. *J. Am. Chem. Soc.* **2011**, *133*, 10612–10620.
6. Rosen, E. L.; Buonsanti, R.; Llordes, A.; Sawvel, A. M.; Milliron, D. J.; Helms, B. A. Exceptionally Mild Reactive Stripping of Native Ligands from Nanocrystal Surfaces by Using Meerwein's Salt. *Angew. Chem., Int. Ed.* **2012**, *51*, 684–689.
7. Chu, I.-H.; Radulaski, M.; Vukmirovic, N.; Cheng, H.-P.; Wang, L.-W. Charge Transport in a Quantum Dot Supercrystal. *J. Phys. Chem. C* **2011**, *115*, 21409–21415.
8. Liu, Y.; Gibbs, M.; Puthussery, J.; Gaik, S.; Ihly, R.; Hillhouse, H. W.; Law, M. Dependence of Carrier Mobility on Nanocrystal Size and Ligand Length in PbSe Nanocrystal Solids. *Nano Lett.* **2010**, *10*, 1960–1969.
9. Lee, J.; Choi, O.; Sim, E. Nonmonotonic Size-Dependent Carrier Mobility in PbSe Nanocrystal Arrays. *J. Phys. Chem. Lett.* **2012**, *3*, 714–719.
10. Segets, D.; Lucas, J. M.; Klupp Taylor, R. N.; Scheele, M.; Zheng, H.; Alivisatos, A. P.; Peukert, W. Determination of the Quantum Dot Band Gap Dependence on Particle Size from Optical Absorbance and Transmission Electron Microscopy Measurements. *ACS Nano* **2012**, *6*, 9021–9032.
11. Moreels, I.; Lambert, K.; De Muynck, D.; Vanhaecke, F.; Poelman, D.; Martins, J. C.; Allan, G.; Hens, Z. Composition and Size-Dependent Extinction Coefficient of Colloidal PbSe Quantum Dots. *Chem. Mater.* **2007**, *19*, 6101–6106.
12. Law, M.; Luther, J. M.; Song, Q.; Hughes, B. K.; Perkins, C. L.; Nozik, A. J. Structural, Optical, and Electrical Properties of PbSe Nanocrystal Solids Treated Thermally or with Simple Amines. *J. Am. Chem. Soc.* **2008**, *130*, 5974–5985.
13. Zarghami, M. H.; Liu, Y.; Gibbs, M.; Gebremichael, E.; Webster, C.; Law, M. p-Type PbSe and PbS Quantum Dot Solids Prepared with Short-Chain Acids and Diacids. *ACS Nano* **2010**, *4*, 2475–2485.
14. Smith, A. R.; Yoon, W.; Heuer, W. B.; Baril, S. I. M.; Boercker, J. E.; Tischler, J. G.; Foos, E. E. Effect of Ligand Structure on the Optical and Electronic Properties of Nanocrystalline PbSe Films. *J. Phys. Chem. C* **2012**, *116*, 6031–6037.
15. Sliem, M. A.; Chemseddine, A.; Bloeck, U.; Fischer, R. A. PbSe Nanocrystal Shape Development: Oriented Attachment at Mild Conditions and Microwave Assisted Growth of Nanocubes. *CrystEngComm* **2011**, *13*, 483–488.
16. Wang, R. Y.; Feser, J. P.; Lee, J.-S.; Talapin, D. V.; Segalman, R.; Majumdar, A. Enhanced Thermopower in PbSe Nanocrystal Quantum Dot Superlattices. *Nano Lett.* **2008**, *8*, 2283–2288.
17. Scheele, M.; Oeschler, N.; Veremchuk, I.; Peters, S.-O.; Littig, A.; Kornowski, A.; Klinke, C.; Weller, H. Thermoelectric Properties of Lead Chalcogenide Core-Shell Nanostructures. *ACS Nano* **2011**, *5*, 8541–8551.
18. Tang, J.; Liu, H.; Zhitomirsky, D.; Hoogland, S.; Wang, X.; Furukawa, M.; Levina, L.; Sargent, E. H. Quantum Junction Solar Cells. *Nano Lett.* **2012**, *12*, 4889–4894.
19. Kang, M. S.; Sahu, A.; Norris, D. J.; Frisbie, C. D. Size- and Temperature-Dependent Charge Transport in PbSe Nanocrystal Thin Films. *Nano Lett.* **2011**, *11*, 3887–3892.
20. Quinn, A. J.; Beecher, P.; Iacopino, D.; Floyd, L.; De Marzi, G.; Shevchenko, E. V.; Weller, H.; Redmond, G. Manipulating the Charging Energy of Nanocrystal Arrays. *Small* **2005**, *1*, 613–618.
21. Laikhtman, B.; Wolf, E. Tunneling Time and Effective Capacitance for Single Electron Tunneling. *Phys. Lett. A* **1989**, *139*, 257–260.
22. Lannoo, M.; Delerue, C.; Allan, G. Screening in Semiconductor Nanocrystallites and Its Consequences for Porous Silicon. *Phys. Rev. Lett.* **1995**, *74*, 3415–3418.
23. Liu, Y.; Tolentino, J.; Gibbs, M.; Ihly, R.; Perkins, C. L.; Liu, Y.; Crawford, N.; Hemminger, J. C.; Law, M. PbSe Quantum Dot Field-Effect Transistors with Air-Stable Electron Mobilities above 7 $cm^2\ V^{-1}\ s^{-1}$. *Nano Lett.* **2013**, *13*, 1578–1587.
24. Choi, H.; Ko, J.-H.; Kim, Y.-H.; Jeong, S. Steric-Hindrance-Driven Shape Transition in PbS Quantum Dots: Understanding Size-Dependent Stability. *J. Am. Chem. Soc.* **2013**, *135*, 5278–5281.
25. Wolcott, A.; Doyeux, V.; Nelson, C. A.; Gearba, R.; Lei, K. W.; Yager, K. G.; Dolocan, A. D.; Williams, K.; Nguyen, D.; Zhu, X.-Y. Anomalously Large Polarization Effect Responsible for Excitonic Red Shifts in PbSe Quantum Dot Solids. *J. Phys. Chem. Lett.* **2011**, *2*, 795–800.
26. Doellefeld, H.; Weller, H.; Eychmueller, A. Particle-Particle Interactions in Semiconductor Nanocrystal Assemblies. *Nano Lett.* **2001**, *1*, 267–269.
27. Kagan, C. R.; Murray, C. B.; Nirmal, M.; Bawendi, M. G. Electronic Energy Transfer in CdSe Quantum Dot Solids. *Phys. Rev. Lett.* **1996**, *76*, 1517–1520.
28. Moreels, I.; Allan, G.; De Geyter, B.; Wirtz, L.; Delerue, C.; Hens, Z. Dielectric Function of Colloidal Lead Chalcogenide Quantum Dots Obtained by a Kramers-Kronig Analysis of the Absorbance Spectrum. *Phys. Rev. B* **2010**, *81*, 235319.
29. Chemla, D. S.; Miller, D. A. B. Mechanism for Enhanced Optical Nonlinearities and Bistability by Combined Dielectric-Electronic Confinement in Semiconductor Microcrystallites. *Opt. Lett.* **1986**, *11*, 522–524.
30. Doellefeld, H.; Weller, H.; Eychmueller, A. Semiconductor Nanocrystal Assemblies: Experimental Pitfalls and a Simple Model of Particle-Particle Interaction. *J. Phys. Chem. B* **2002**, *106*, 5604–5608.
31. Geiregat, P.; Justo, Y.; Abe, S.; Flamee, S.; Hens, Z. Giant and Broad-Band Absorption Enhancement in Colloidal Quantum Dot Monolayers through Dipolar Coupling. *ACS Nano* **2013**, *7*, 987–993.
32. Sykora, M.; Koposov, A. Y.; McGuire, J. A.; Schulze, R. K.; Tretiak, O.; Pietryga, J. M.; Klimov, V. I. Effect of Air Exposure on Surface Properties, Electronic Structure, and Carrier Relaxation in PbSe Nanocrystals. *ACS Nano* **2010**, *4*, 2021–2034.
33. Gautier, C.; Cambon-Muller, M.; Averous, M. Study of PbSe Layer Oxidation and Oxide Dissolution. *Appl. Surf. Sci.* **1999**, *141*, 157–163.
34. Zhang, J.; Kumbhar, A.; He, J.; Das, N. C.; Yang, K.; Wang, J.-Q.; Wang, H.; Stokes, K. L.; Fang, J. Simple Cubic Super Crystals Containing PbTe Nanocubes and Their Core-Shell Building Blocks. *J. Am. Chem. Soc.* **2008**, *130*, 15203–15209.
35. Weber, M. J. *Handbook of Optical Materials*; CRC Press, 2003.
36. da Silva, A. F.; Pepe, I.; Persson, C.; de Almeida, J. S.; Araújo, C. M.; Ahuja, R.; Johansson, B.; An, C. Y.; Guo, J.-H. Optical Properties of Oxide Compounds PbO, SnO_2, and TiO_2. *Phys. Scr.* **2004**, *2004*, 180–183.